Anal. Chem. **2000,** *72,* 1156−1162

Electrostatic Axially Harmonic Orbital Trapping: A High-Performance Technique of Mass Analysis

Alexander Makarov*

HD Technologies Ltd., Atlas House, Simonsway, Manchester, M22 5PP, U.K.

This work describes a new type of mass analyzer which employs trapping in an electrostatic field. The potential distribution of the field can be represented as a combination of quadrupole and logarithmic potentials. In the absence of any magnetic or rf fields, ion stability is achieved only due to ions orbiting around an axial electrode. Orbiting ions also perform harmonic oscillations along the electrode with frequency proportional to $(m/z)^{-1/2}$. These oscillations are detected using image current detection and are transformed into mass spectra using fast FT, similarly to FT ICR. Practical aspects of the trap design are presented. High-mass resolution up to 150 000 for ions produced by laser ablation has been demonstrated, along with high-energy acceptance and wide mass range.

Recent years have firmly established ion trapping techniques as very important tools of mass spectrometry. Widespread acceptance of Paul's trap[1] as well as increasing use of FT ICR[2] creates a first impression that these two complementary trapping techniques could cover all needs of organic and biomolecular mass spectrometric analysis. Closer analysis, however, reveals concerns about the insufficient mass accuracy of Paul's trap and the high complexity and cost of FT ICR, as well as the relatively low space charge capacity of both.[1,3] Practical difficulties of rectifying these drawbacks indicate the necessity of fresh approaches to ion trapping.

This work proposes that dynamic ion trapping in electrostatic fields may be such an approach. Three types of dynamic trapping are known: linear, segmented ring, and orbital.

In linear trapping, ions are introduced and trapped between two ion mirrors coaxial to the ion beam. To introduce ions, one of the mirrors is switched off to transmit the ions from the ion source, and then it is switched on before the ions of interest return from the second mirror. In mass spectrometry, such trapping has been used for experiments involving narrow mass range time-of-flight mass spectrometry[4−6] or single-ion analysis.[7] The complexities of both the construction and the associated electronics even for modest mass resolution are to be held responsible for the slow progress of this approach.

In segmented-ring trapping, multiple electrostatic sectors forming a full circle are used instead of the mirrors.[4] Ions move along arcs inside the sectors and along straight lines between them. For ion injection, one of the sectors is switched off. This type of trapping is very typical for studying the physics of elementary particles (ring accelerators[8]). It has been also used for narrow mass range time-of-flight mass spectrometry.[9] The complexity of the associated experimental setup is even higher than that for linear trapping.

Orbital trapping was first implemented by Kingdon in 1923.[10] In its classical shape, the Kingdon trap contains a wire stretched along the axis of an outer cylinder with flanges enclosing the trapping volume. When a voltage is applied between the wire and the cylinder, the strong field attracts ions to the wire. Only ions that have enough tangential velocity miss the wire and survive. In some way, their orbits are similar to orbits of planets or asteroids in the Solar system, the wire playing the role of the Sun. Motion along the wire is restrained by the field curvature caused by the flanges of the outer cylinder. Further variations of the Kingdon trap are known, for example, with two parallel wires[11] or more elaborate electrode shapes ("ideal Kingdon trap" [12]).

Orbital trapping has been widely used in experiments on the spectroscopy of ions.[12−15] In these applications, ions have been formed within the trap or injected tangentially prior to switching on the field of the trap. The Kingdon trap has been also used as the cell for FT ICR[16] though within the framework of a traditional FT ICR experiment. Recently it has been proposed[17] to use the Kingdon trap as a self-contained mass spectrometer with image

(1) March, R. E. *Rapid Commun. Mass Spectrom.* **1999**, *13*, 1543−1554.
(2) Dienes, T.; Pastor, S. J.; Schurch, S.; Scott, J. R.; Yao, J.; Cui, S.; Wilkins, C. L. *Mass Spectrom. Rev.* **1996**, *15*, 163-211.
(3) Easterling, M. L.; Mize, T. H.; Amster, I. J. *Anal. Chem.* **1999**, *71*, 624−632.
(4) Wollnik, H. *Int. J. Mass Spectrom. Ion Processes* **1994**, *131*, 387−407.
(5) Dahan, M.; Fishman, R.; Heber, O.; Rappaport M.; Altstein N.; Zajfman D.; van der Zande W. J. *Rev. Sci. Instrum.* **1998**, *69*, 76−83.
(6) Piyadasa, C. K.; Hakansson, P.; Ariyarathe, T. R. *Rapid Commun. Mass Spectrom.* **1999**, *13*, 620−624.
(7) Benner, H. W. *Anal. Chem.* **1997**, *69*, 4162−4169.
(8) Bryant, P.; Johnsen, K. *The principles of circular accelerators and storage rings*; Cambridge University Press: Cambridge, 1993.
(9) Sakurai, T.; Nakabushi, H.; Hiasa, T.; Okanishi K. *Nucl. Instrum. Methods* **1999**, *A427*, 182−186.
(10) Kingdon, K. H. *Phys. Rev.* **1923**, *21*, 408−418.
(11) McIlraith, A. H. *Nature* **1966**, *212*, 1422−1424.
(12) Knight, R. D. *Appl. Phys. Lett.* **1981**, *38*, 221−222.
(13) Lewis, R. R. *J. Appl. Phys.* **1982**, *53*, 3975−3980.
(14) Yang, L.; Church, D. A. *Nucl. Instrum. Methods Nucl. Res.* **1991**, *B56/57*, 1185−1187.
(15) Sekioka, T.; Terasama, M.; Awaya, Y. *Rad. Effects Defects Solids* **1991**, *117*, 253−259.
(16) Gillig, K. J.; Bluhm, B. K.; Russell, D. H. *Int. J. Mass Spectrom. Ion Processes* **1996**, *157/158*, 129−147.
(17) Oksman P. *Int. J. Mass Spectrom. Ion Processes* **1995**, *141*, 67−76.

10.1021/ac991131p CCC: $19.00
Published on Web 02/10/2000

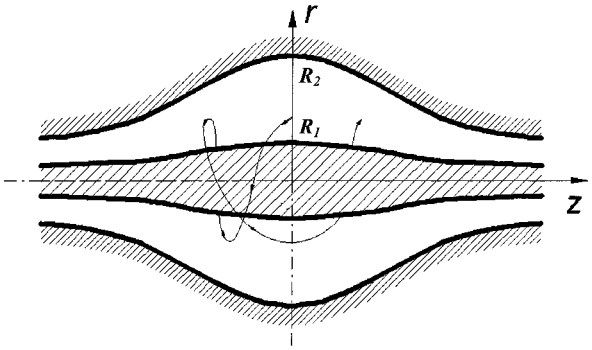

Figure 1. Equipotentials of the quadro-logarithmic field and an example of a stable ion trajectory

current detection. However, it had been planned to derive the mass-to-charge ratio from the frequency of ion rotation. Due to the strong dependence of the rotation frequency on ion velocity and initial radius, this approach leads to poor mass resolution.

In this work, the concept of orbital trapping is freshly revised for application to mass analysis. A new type of mass analyzer is described which employs orbital trapping in an electrostatic field with potential distribution:[12,16,18]

$$U(r,z) = \frac{k}{2}\left(z^2 - \frac{r^2}{2}\right) + \frac{k}{2}(R_m)^2 \ln\left[\frac{r}{R_m}\right] + C \qquad (1)$$

where r and z are cylindrical coordinates ($z = 0$ being the plane of the symmetry of the field), C is a constant, k is field curvature, and R_m is the characteristic radius. This field is the sum of a quadrupole field of the ion trap and a logarithmic field of a cylindrical capacitor; therefore, it may be also called a quadro-logarithmic field.

The main distinction of the this trap is that mass-to-charge ratio is derived from the frequency of harmonic ion oscillations *along the axis* of the field (1).[19] This axial frequency may be determined using image current detection and fast FT algorithms.[2] Use of the axial frequency as opposed to rotational or radial frequency is essential because only this frequency is completely independent of energy and spatial spread of ions (see below). A mass analyzer employing such electrostatic axially harmonic orbital trapping is referred hereinafter as the orbitrap.

The potential advantages of the orbitrap include the following: (1) high mass resolution (up to 100 000−200 000) since the field (1) may be defined with very high accuracy; (2) increased space charge capacity at higher masses due to independence of trapping potential on mass-to-charge ratio and larger trapping volume—in contrast to FT ICR and Paul's trap; (3) high mass accuracy, dynamic range, and upper mass limit due to the factors listed above.

THEORETICAL SECTION

Geometry of the Orbitrap. The trap consists of an outer barrel-like electrode and a central spindle-like electrode along the axis (Figure 1). The shape of these axially symmetrical electrodes could be deduced from eq 1:

$$z_{1,2}(r) = \sqrt{\frac{r^2}{2} - \frac{(R_{1,2})^2}{2} + (R_m)^2 \ln\left[\frac{R_{1,2}}{r}\right]} \qquad (2)$$

where index 1 denotes the central electrode, index 2 denotes the outer electrode, $z = 0$ is the plane of symmetry, and $R_{1,2}$ are the maximum radii of the corresponding electrodes.

Ion Trajectories. In the field (1), stable trajectories combine rotation around the central electrode with oscillations along the axis, resulting in an intricate spiral. Equation of motion in polar coordinates (r, φ, z) for ions with mass-to-charge ratio m/q are

$$\left.\begin{aligned} &\ddot{r} - r\dot{\varphi}^2 = -\frac{q}{m}\frac{k}{2}\left[\frac{(R_m)^2}{r} - r\right] && \text{(a)} \\ &\frac{\mathrm{d}}{\mathrm{d}t}(r^2\dot{\varphi}) = 0 && \text{(b)} \\ &\ddot{z} = -\frac{q}{m}kz && \text{(c)} \end{aligned}\right\} \qquad (3)$$

with initial conditions at the moment $t = 0$

$$\begin{aligned} r(0) &= r_0 \qquad \dot{r}(0) = \dot{r}_0 \\ \varphi(0) &= \varphi_0 \qquad \dot{\varphi}(0) = \dot{\varphi}_0 \\ z(0) &= z_0 \qquad \dot{z}(0) = \dot{z}_0 \end{aligned} \qquad (4)$$

Equation 3a reveals the physical meaning of the characteristic radius R_m. If $r < R_m$, the electric field attracts ions to the axis and repels otherwise. For trapping, only radii below R_m are useful.

According to (3), motion in the polar plane (r, φ) is completely independent of the motion along z. Also, $\dot{\varphi}$ could be excluded from (3a) using (3b). Therefore, it is convenient to introduce separate energy characteristics E_r, E_φ, E_z for each direction:

$$\begin{aligned} qE_r &= (m/2)(\dot{r}_0)^2 \\ qE_\varphi &= (m/2)(r_0\dot{\varphi}_0)^2 \\ qE_z &= (m/2)(\dot{z}_0)^2 \end{aligned} \qquad (5)$$

and the ion initial kinetic energy is the sum of all three.

The equation of motion along z (3c) describes a simple harmonic oscillator and its exact solution is

$$z(t) = z_0 \cos(\omega t) + \sqrt{(2E_z/k)}\,\sin(\omega t) \qquad (6)$$

where

$$\omega = \sqrt{(q/m)k} \qquad (7)$$

is the frequency of axial oscillations (in rad/s).

For the polar plane (r, φ), eqs 3a and 3b cannot be integrated analytically. In the general case, they define a trajectory looking like a rotating ellipse. To reduce the influence of field imperfec-

(18) Gall, L. N.; Golikov, Y. K.; Aleksandrov, M. L.; Pechalina, Y. E.; Holin, N. A. USSR Inventor's Certificate 1247973, 1986.
(19) Makarov A. A. U.S. Pat*ent* 5,886,346, 1999.

tions on the frequency of ion oscillations, it is preferable to have this ellipse as close to a circle as possible. The circular shape of the trajectory is achieved when $E_r = 0$ and E_φ equals $\tilde{E}_\varphi$, where

$$\tilde{E}_\varphi = (k/4)((R_\mathrm{m})^2 - R^2) \tag{8}$$

where R is radius of the circle and eq 8 is obtained from (3) for $\dot{r} = \ddot{r} = 0$. For trajectories close to circular, equations of motion could be solved approximately by using any of the available aberration theories (the method of τ-variations[20] has been used in this work). In the first approximation, the solution is

$$r(t) = R + (r_0 - R)[\eta + (1 - \eta)\cos(\omega_r t)] + \sqrt{\frac{\eta}{2}\frac{E_r}{\tilde{E}_\varphi}}R\sin(\omega_r t) + \frac{E\varphi - \tilde{E}\varphi}{\tilde{E}_\varphi}\frac{\eta}{2}R(1 - \cos(\omega_r t))$$

$$\varphi(t) = \omega_\varphi t\left[1 + \frac{r_0 - R}{R}(1 - 2\eta)\right] + \frac{E\varphi - \tilde{E}\varphi}{\tilde{E}_\varphi}\left(\frac{1}{2} - \eta\right)t + \varphi_0 + \vartheta \tag{9}$$

where ϑ represents the sum of all oscillating terms (negligible for $t \gg 1/\omega_r$),

$$\eta = 1 + \frac{1}{(R_m/R)^2 - 2}$$

ω_r is the frequency of radial oscillations:

$$\omega_r = \sqrt{\frac{q}{m}k}\sqrt{\left(\frac{R_m}{R}\right)^2 - 2} = \omega\sqrt{\left(\frac{R_m}{R}\right)^2 - 2} \tag{10}$$

and ω_φ is the frequency of rotation:

$$\omega_\varphi = \frac{1}{R}\sqrt{\frac{2q}{m}\tilde{E}\varphi} = \omega\sqrt{\frac{\left(\frac{R_m}{R}\right)^2 - 1}{2}} \tag{11}$$

As was noted above, the electric field attracts ions to the axis for $R < R_m$ and this condition is usually sufficient to trap ions with small $E\varphi$: $E_\varphi \ll \tilde{E}_\varphi$. However, for ions with $E\varphi$ close to $\tilde{E}_\varphi$, ($E_\varphi - \tilde{E}_\varphi$) $\ll \tilde{E}_\varphi$, expression 10 indicates that attractive electric force starts to exceed repulsive centrifugal force caused by circular rotation only at radii $R < R_m/2^{1/2}$, otherwise radial oscillations become unstable. For $E_\varphi > \tilde{E}_\varphi$, even lower R are required for ion stability.

Out of three characteristic frequencies ω_r, ω_φ, ω introduced above, only axial frequency ω is completely independent of the energy and the position of ions. Therefore, only this frequency could be used for mass analysis. This is how the "ideal Kingdon trap" becomes a mass analyzer—the orbitrap.

Image Current Detection. In this mode, image current is detected on split outer electrodes and amplified by a differential amplifier (Figure 2a). The signal voltage induced by ion oscillations may be obtained using Green's reciprocity theorem.[21] The theorem provides the relationship between image charge Q induced on the electrodes by a charge q at a point (r, φ, z), and potential change $\Delta\Phi(r, \varphi, z)$ induced in the same point by voltage ΔU applied to the same electrodes in the absence of any charge:

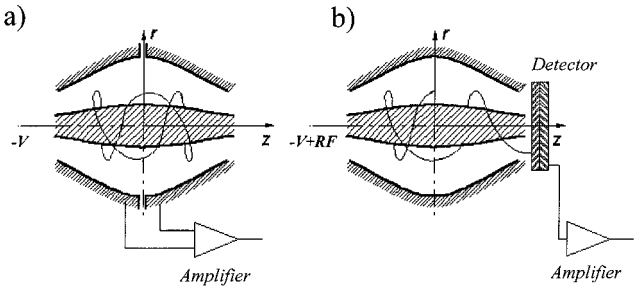

Figure 2. Modes of mass analysis in the orbitrap: (a) Fourier transform mass spectrometry (image current detection); (b) mass-selective instability (detection using secondary electron multiplier).

$$Q/q = -(\Delta\Phi(r,\varphi,z)/\Delta U) \tag{12}$$

Due to axial symmetry of electrodes, potential $\Delta\Phi$ in (12) does not depend on angle φ. Then differential image current on the detection electrodes is

$$I(t) = \frac{\mathrm{d}Q}{\mathrm{d}t} = -\frac{q}{\Delta U}\left[\frac{\partial\Delta\Phi(r,z)}{\partial r}\dot{r} + \frac{\partial\Delta\Phi(r,z)}{\partial z}\dot{z}\right] \tag{13}$$

For a cloud of ions, total image current will be the sum of individual currents given by (13). It means that $\dot{r}$ and $\dot{z}$ will be averaged. This is where properties of ion radial and axial motion become important. If ions are initially all displaced from a circular trajectory in the equator plane (i.e., excited), they will continue to oscillate along z together, in-phase due to the independence of axial frequency on ion energy or ion position. Contrary to this, the frequency of radial motion will be slightly different for ions with different r_0, E_r, E_φ. It means that in the radial direction ions will go out of phase with each other orders of magnitude faster than in the axial direction. Therefore, the presence of side bands and mixed harmonics in the frequency spectrum associated with radial oscillations could be made insignificant just by allowing a relatively small delay prior to ion detection. Then for a cloud of N ions excited to amplitude Δz and rotating around the central electrode at *average* radius ρ, total image current is approximately

$$I(t) \approx -\frac{q}{\Delta U}N\frac{\partial\Delta\Phi(r,0)}{\partial z}\dot{z} \approx -qN\omega\frac{\Delta z}{\lambda}\sin(\omega t) \tag{14}$$

where λ is "effective gap" between detection electrodes. Due to the complex geometry of the trap, this parameter depends on ρ as exemplified in Figure 3. This dependence may be made much weaker if the central electrode is also split and used for ion detection.

(20) Kolesnikov, S. V.; Monastyrskii, M. A. *Sov. Phys. Technol. Phys.* **1988**, *33*, 1−11.

(21) Marto, J. A.; Marshall, A. G.; Schweikhard, L. *Int. J. Mass Spectrom. Ion Processes* **1994**, *137*, 9−30.

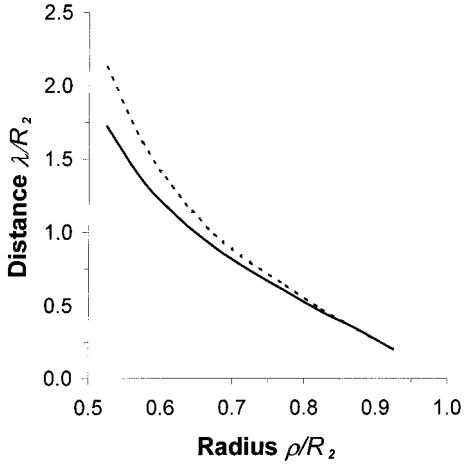

Figure 3. Dependence of "effective gap" λ on average radius of trajectories ρ ($R_1/R_2 = 0.35$) for infinite length of detection electrodes (solid line) and for detection electrodes of length $L = 0.5 \cdot R_2$ (dashed line).

The image current is amplified and processed exactly in the same way as in FT ICR;[21−22] therefore, similar sensitivity and signal-to-noise ratios are expected. The resulting frequency spectrum however differs due to a much slower decrease of ion frequency with mass according to (7). In this aspect, the orbitrap reveals its kinship to a time-of-flight mass spectrometer. As a result, the mass resolution of the orbitrap in FT MS mode is twice lower than the frequency resolution:

$$M/\delta M = (1/2)(\omega/\delta\omega) \qquad (15)$$

Mass-Selective Instability. Mass-selective instability mode is an alternative mode of mass analysis in the orbitrap. In this mode, radio frequency (rf) voltage is added to the static voltage on the central electrode (Figure 2b). In eqs 3a and 3c, it results in the modulation of their right parts with rf frequency. Then motion along z is governed by the canonical Mathieu equation while the equation for radial motion becomes even more complex and nonlinear. Mathieu parameters a_u and q_u could be introduced for the axial motion:[23]

$$a_u = 4(\omega^2/\Omega^2) \qquad q_u = 2\mu(\omega^2/\Omega^2) \qquad (16)$$

where Ω is the angular frequency of the rf field (in rad/s) and μ is the ratio of the rf amplitude (0 − p) to the average voltage between central and outer electrodes of the trap.

The peculiarity of the orbitrap is that the nonlinearity of the radial oscillations allows it to operate in a unique region of the stability diagram (Figure 4). At low rf voltages (i.e., low q_u), parametric resonance along r and the excitation of the radial oscillations may develop for at least some ions. Fortunately, this process appears to be self-quenching due to very strong nonlinearity of the radial oscillations.[24]

(22) Anderson, G. A.; Bruce, J. E.; Hofstadler, S. A.; Rockwood, A. L.; Smith, R. D. *Proc. 43rd ASMS Conf. Mass Spectrom. Allied Top.*, Atlanta, GA, May 21−26, 1995; p1093.

(23) March, R. E.; Hughes R. J. *Quadrupole Storage Mass Spectrometry*; Wiley-Interscience: New York, 1989.

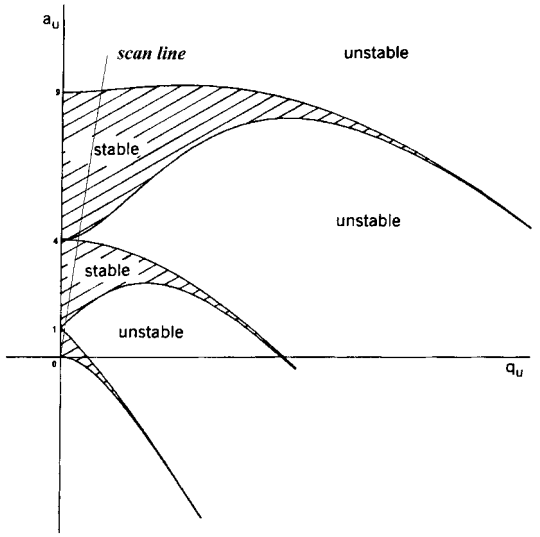

Figure 4. Stability diagram of the Mathieu equation (axial direction) and the scan line of the orbitrap in mass-selective instability mode.

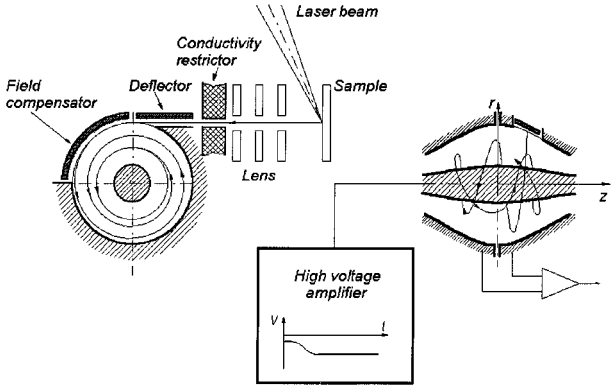

Figure 5. Schematics of experimental setup (side view and front view).

For axial oscillations, parametric resonance develops when $a_u \rightarrow 1$ for ions with specific m/q (i.e., $\Omega = 2\omega$, $q_u = \mu/2$). The axial coordinate of the ions increases rapidly until they are ejected to the detector along the axis of the orbitrap (Figure 2c). Unlike Paul's trap,[1] just several volts of rf will be enough for any mass.

EXPERIMENTAL SECTION

The experimental setup is represented schematically in Figure 5. Electrodes of the trap have been machined from stainless steel using a numerically controlled high-precision lathe to the shape described by (2) and shown in Figure 2a with $R_1 = 7$ mm and $R_2 = 20$ mm. Ions are formed by a pulsed nitrogen laser (Laser Science Inc., Franklin, MA) focused on the flat tip of the stainless steel probe. These ions are accelerated by a voltage drop of 1.1−1.2 kV across a 10 mm acceleration gap. After that, they enter an accelerating electrostatic lens formed by two grounded apertures and one aperture between them. All apertures are 5 mm i.d., 2 mm thick, and equispaced by 6 mm. This lens focuses the ion beam into a 1 mm i.d., 10 mm long conductivity restrictor separating the internal trap volume from the exterior. After the conductivity restrictor, a miniature deflector is positioned in order

(24) Mitropol'skii, Y. A. *Problems of the Asymptotic Theory of Nonstationary Vibrations*; Daniel Davey: New York, 1965.

to optimize the entrance angle of the ion beam. Ions enter the trap through a narrow ion injection channel tangentially to the outer electrode (Figure 5). An additional electrode with adjustable voltage is used as a field compensator to minimize three-dimensional field distortion introduced by the ion injection channel.

To increase the mass range of trapped ions, the principle of electrodynamic squeezing has been developed.[19] According to this principle, ions enter the field tangentially to the outer electrode and are prevented from hitting this electrode again by a monotonically increasing electric field, which squeezes them closer to the center of the trap, like stars to a black hole. The time constant of the electric field increase depends on the mass range to be trapped and usually stays within 20−100 μs. Squeezing stops as soon as there is no more threat of losing ions on the electrodes. As the detection electrodes are kept at virtual ground, only the voltage on the central electrode is monotonically changed down to −5 kV by a home-built high-voltage amplifier synchronized with the laser pulse. The final kinetic energy of trapped ions after electrodynamic squeezing is estimated to be around 2.2 kV.

So far, all experiments have been confined to the FT MS-only mode. In the present "proof-of-principle" setup, all-mass excitation for image current detection has been performed simply by off-equator tangential injection of ions ("excitation by injection"). Coherence of ion motion is achieved due to the small dimenisions of the ion packets on entrance to the trap.

Detection starts after the voltage on the central electrode reaches a steady state, usually after 20−90 ms. Image current from the detection electrodes is amplified by a differential preamplifier,[22] courtesy of Pacific Northwest National Laboratory, and is Fourier transformed using a home-built board with 1.25 MHz 9 bit ADC and 1 Mbyte record length. If this record length is not sufficient, digital oscilloscope LC584AL (LeCroy Inc., Chestnut Ridge, NY) with an 8 MB record length is used. No conditioning of the data (e.g., zero filling) has been used. To improve the signal-to-noise ratio in MALDI experiments, individual spectra in the frequency domain were added together.

The trap, ion source, and sample introduction unit are located inside a small main vacuum chamber (290 mm long, 140 mm high, 160 mm wide) sustained at a pressure of 2×10^{-7} mbar by a 70 L/s turbo pump backed by a 1.5 m^3/h rotary pump (Edwards Ltd., Crawley, U.K.). The interior volume of the trap is pumped down to 10^{-9}−10^{-10} mbar (measured on the pump) by a 40 L/s ion pump (Physical Electronics, Eden Prairie, MN). The entire setup forms a compact benchtop unit (600 mm wide, 600 mm high, 500 mm deep).

Samples for experiments with atomic ions have been prepared by depositing 1 μL of a saturated NaCl or CsI salt solution on the tip of the stainless steel probe. Tin/lead alloy has been atttached to the probe by soldering with acid flux. Samples for MALDI analysis were prepared using a direct deposition method by placing 1 μL of a 10 μM poly(ethylene) glycol (PEG-1000) polymer standard or angiotensin-2 solution on the probe followed by 1 μL of a saturated solution of 2,5-dihydroxybenzoic acid (DHB).

RESULTS AND DISCUSSION

A typical recorded transient of atomic ions is represented in Figure 6. It corresponds to approximately 2×10^5 ions injected into the trap. Figure 6 shows that the signal remains detectable for more than 0.5 s (detection stops after 0.8 s). The decay of the transient speeds up if pressures exceed $(2-5) \times 10^{-8}$ mbar as measured on the ion pump. Also, signal decay is dramatically accelerated if voltages on the compensation electrodes or the shape of the electrodes perturbs the field (1).

Figure 6. Typical transient for $^{56}Fe^+$. Hundreds of thousands of oscillations merge into the black envelope.

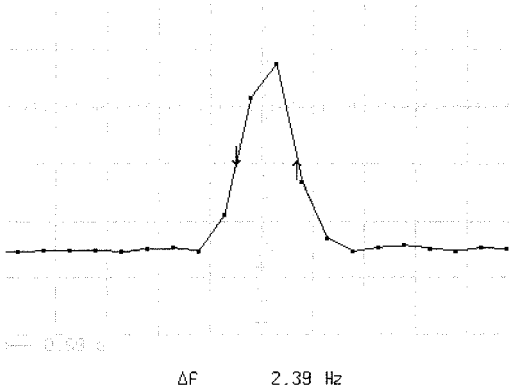

Figure 7. Mass peak of $^{56}Fe^+$ in the frequency domain (peak centroid is at 711 kHz).

When the transient of Figure 6 is transformed, it yields the frequency spectrum shown in Figure 7. No significant side bands or higher harmonics have been observed. Peak shape stays the same even if the ion energy is changed by more than ±5%, which is approximately 100 eV. Peak width is 2.39 Hz at a frequency 711 kHz, which corresponds to a full-width half-maximum (fwhm) frequency resolution of about 300 000 and a mass resolution of 150 000. These experiments with atomic ions are important for finding at what level mass resolution is limited primarily by the construction itself rather than by pressure or metastable decay. Mass analysis of a broad range of masses and concentrations is also possible as shown in Figure 8 for a tin/lead 60:40 mixture. Though the response is dependent on the element (as it is usual for laser ablation), isotopic ratios measured in individual shots appear to be within ±5−10% of the correct ratio. Only the smallest isotopes (below a few percent) were found to be discriminated against, presumably due to the low dynamic range of the electronics.

Results of experiments on mass accuracy and the calibration curve of the orbitrap are represented in Figure 9. Data were acquired over more than 20 h using laser ablation of a mixed salt sample. The spread of signal intensities within this series of measurements has been more than a factor of 10. The frequency of $^{133}Cs+$ has been used to find k in (7), and then the mass of

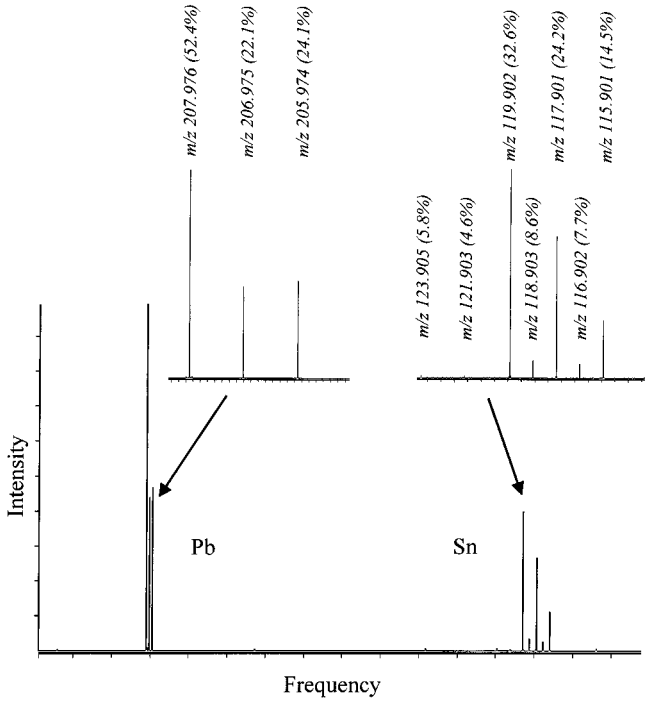

Figure 8. Panoramic mass spectrum of laser-ablated solder alloy (40%:60% lead/tin) in the frequency domain. Accurate masses of most abundant isotopes are shown along with their natural abundance.

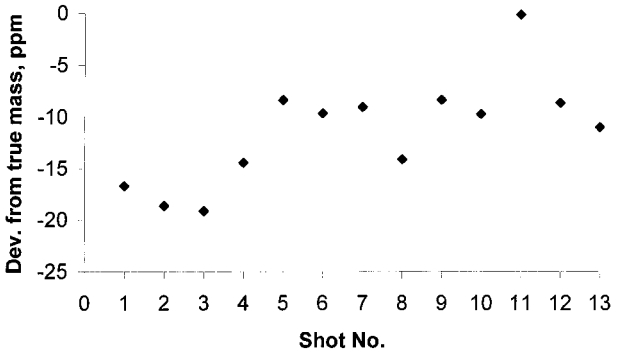

Figure 9. Measured mass of $^{23}Na^+$ for individual laser shots over 20 h. $^{133}Cs^+$ has been used as the only internal calibrant.

$^{23}Na^+$ has been calculated from (7) according to the measured frequency. The calculated mass is only 11 ppm from the theoretical mass, although it is almost 6 times different. The root-mean-square deviation for *individual shots* is 5 ppm.

MALDI experiments resulted in the frequency-domain spectra of Figures 10 and 11. Isotopic resolution and reasonable isotopic ratios have been achieved for a PEG-1000 standard (Figure 10) as well as for angiotensin-2 (Figure 11). It should be noted that these figures represent mass spectra in the frequency domain so higher mass isotopes appear to the left. Unfortunately, much faster signal decay has been observed for these polyatomic ions, with the time constant of ~20−30 ms for PEG-1000 and ~10−20 ms for angiotensin-2. Due to the independence of pressure, the effect has been attributed to metastable fragmentation that is consistent with the experience of MALDI FT ICR[25] (when no cooling is used).

Figure 10 demonstrates a broad distribution of PEG oligomers without any mass discrimination relative to typical MALDI spectra

(25) Castoro, J. A.; Wilkins, C. L. *Anal. Chem.* **1993**, *65*, 2621−2627.

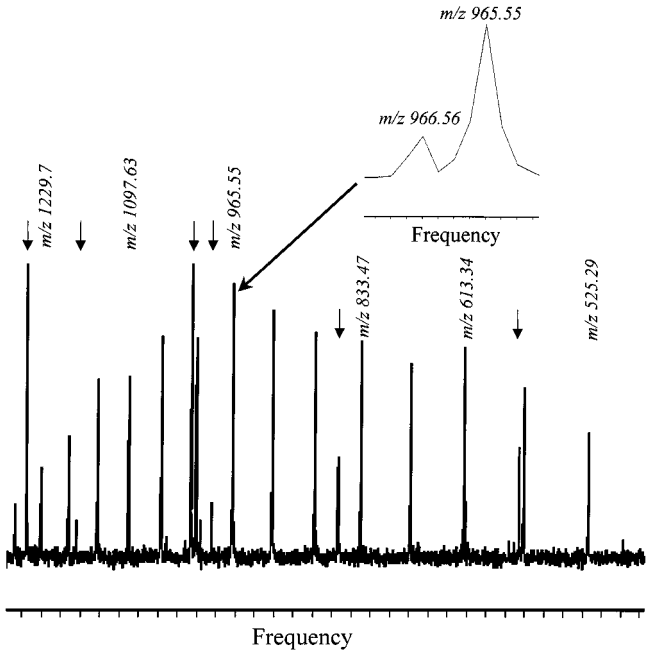

Figure 10. Wide mass range spectrum of PEG-1000 in the frequency domain (sum of 30 laser shots). Noise peaks of electronics are marked by arrows while all other peaks represent oligomers of PEG-1000. The most intense mass peak of the distribution (at mass 966.55 Da) is shown in detail in the inset.

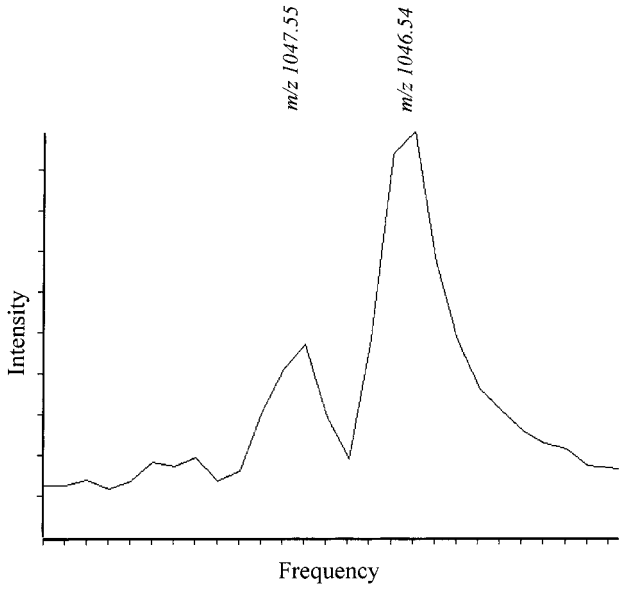

Figure 11. Mass spectrum of angiotensin-2 in the frequency domain (sum of 30 laser shots).

of the PEG-1000 polymer standard. It means that the range of masses simultaneously injected and trapped in the orbitrap is quite wide. Indeed, this spectrum was acquired at the same settings as the spectra for atomic ions. It means that the use of electrodynamic squeezing allows trapping of a wide mass range with $M_{max}/M_{min} > 50$. To increase the upper mass limit M_{max}, it will be necessary simply to increase the rise time of the high-voltage amplifier (Figure 5). Figure 10 also shows several noise peaks (marked by arrows) which are effectively higher harmonics of switching frequencies of dc−dc converters inside the high-voltage amplifier and power supplies.

CONCLUSIONS

These results show that the orbitrap is a new and effective mass spectrometer which could potentially find its own unique niche. With mass resolution surpassed only by FT ICR, the orbitrap has the advantage of a much simpler and compact design.

To become useful for the main stream of mass spectrometric analysis, the orbitrap requires external collisional cooling and possibly external ion accumulation. These goals become the main priorities of further development work.

ACKNOWLEDGMENT

The invaluable role of Andrew Hoffmann, Robert Lawther, Stephen Davis, Nick Demetriades, and Jonathan Hughes (HD Technologies Ltd.) in the practical realization of the orbitrap is gratefully acknowledged. The author also thanks Gordon Anderson and Mike Belov (Pacific Northwest National Laboratory) for their help with the image current preamplifier, Michail Monastyrsky and Victor Tarasov (Institute of General Physics, Moscow) for their help with numerical methods, and Jae Schwartz and Mike Senko (ThermoQuest, San Jose) for their comments on the manuscript. The development was partly supported by a U.K. Department of Trade and Industry SMART award.

Received for review September 29, 1999. Accepted December 20, 1999.

AC991131P